

You Only Hypothesize Once: Point Cloud Registration with Rotation-equivariant Descriptors

Haiping Wang*
Wuhan University
Wuhan, Hubei, China
hpwang@whu.edu.cn

Yuan Liu*
The University of Hong
Kong
Hong Kong, China
yliu@cs.hku.hk

Zhen Dong†
Wuhan University
Wuhan, Hubei, China
dongzhenwhu@whu.edu.cn

Wenping Wang
Texas A&M University
College Station, Texas, USA
wenping@tamu.edu

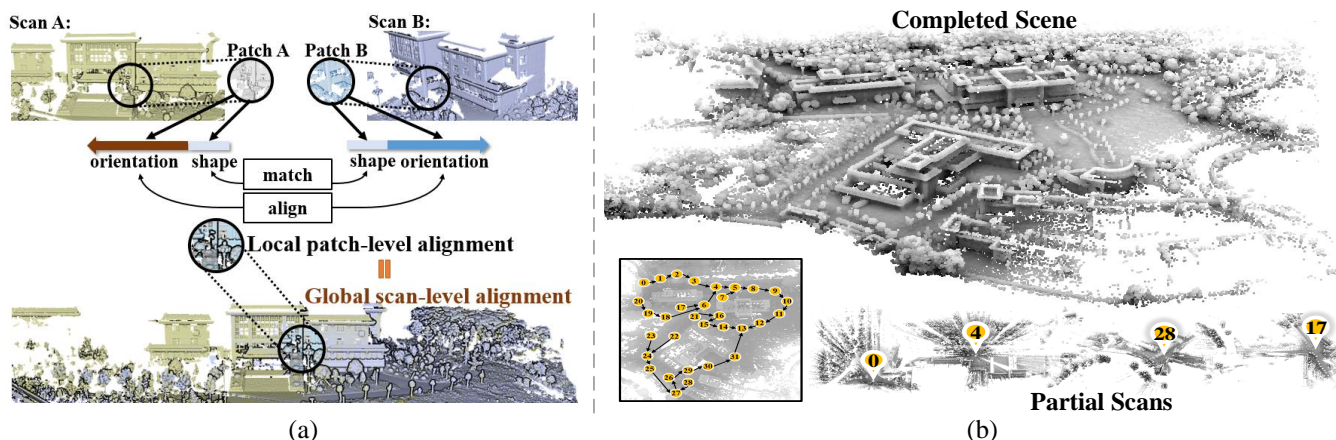


Figure 1: We present a novel framework called YOHO for point cloud registration. (a) The key idea of YOHO is to utilize orientations of local patches to find the global alignment of partial scans. (b) YOHO is able to automatically integrate partial scans into a completed scene, even these partial scans contain lots of noise and significant point density variations.

ABSTRACT

In this paper, we propose a novel local descriptor-based framework, called You Only Hypothesize Once (YOHO), for the registration of two unaligned point clouds. In contrast to most existing local descriptors which rely on a fragile local reference frame to gain rotation invariance, the proposed descriptor achieves the rotation invariance by recent technologies of group equivariant feature learning, which brings more robustness to point density and noise. Meanwhile, the descriptor in YOHO also has a rotation-equivariant part, which enables us to estimate the registration from just one correspondence hypothesis. Such property reduces the searching space for feasible transformations, thus greatly improving both the accuracy and the efficiency of YOHO. Extensive experiments show that YOHO achieves superior performances with much fewer needed RANSAC iterations on four widely-used datasets, the 3DMatch/3DLoMatch datasets, the ETH dataset and the WHU-TLS

dataset. More details are shown in our project page: <https://hpwang-whu.github.io/YOHO/>.

CCS CONCEPTS

• **Theory of computation** → **Computational geometry**; • **Computing methodologies** → **Matching**; **Shape modeling**.

KEYWORDS

3D Registration; Point Cloud Registration; Scene Reconstruction; Rotation Equivariance; Shape Descriptor

ACM Reference Format:

Haiping Wang, Yuan Liu, Zhen Dong, and Wenping Wang. 2022. You Only Hypothesize Once: Point Cloud Registration with Rotation-equivariant Descriptors. In *Proceedings of the 30th ACM International Conference on Multimedia (MM '22)*, Oct. 10–14, 2022, Lisboa, Portugal. ACM, New York, NY, USA, 12 pages. <https://doi.org/10.1145/3503161.3548023>

1 INTRODUCTION

Finding an accurate $SE(3)$ transformation of two unaligned partial point clouds, known as point cloud registration, is a prerequisite for many tasks such as 3D reconstruction [28, 46, 54, 85], pose estimation [2, 30, 45, 82], AR/VR [29, 50, 71, 83], and autonomous driving [8, 53, 74, 80]. Due to the large searching space of $SE(3)$, directly finding an accurate transformation by enumerating is infeasible. A commonly-used pipeline usually consists of first extracting

*Both authors contributed equally to this research.

†The corresponding author.



This work is licensed under a Creative Commons Attribution International 4.0 License.

local descriptors of some interest points and then matching these local descriptors to build a set of putative correspondences. Hence, the searching space is only limited to $SE(3)$ transformations that can explain the putative correspondences. However, due to noise and density variations in point clouds, the putative correspondences often contain lots of false correspondences so that the searching space still remains too large to find a correct transformation.

In order to establish reliable correspondences, the local descriptor needs to be invariant to the rotation brought by the unknown $SE(3)$ transformation. To achieve such invariance, most existing works [3, 31] align different interest points with local reference frames (LRF) constructed by principle component analysis (PCA) [72]. However, such a LRF construction is ambiguous [40] and usually sensitive to noise and point density as shown in Fig. 2, which may produce a completely incorrect alignment between two corresponding points. The incorrect alignment poses a great challenge for the subsequent feature extraction to find a rotation-invariant descriptor. Some other works [17, 18, 56] resort to handcrafted rotation-invariant features like point-pair angles or distances to construct a descriptor. However, these handcrafted features usually discard many useful geometry information thus are less discriminative. Recent technologies [10, 13, 14, 26, 51, 65] of extracting features on the $SO(3)$ or $SE(3)$ group brings potentials for directly learning a rotation-invariant descriptor from raw point clouds, which takes good advantage of the powerful representation ability of neural networks to learn discriminative and rotation-invariant descriptors.

Though the nonalignment of two corresponding points poses a requirement of rotation invariance, it also provides an opportunity to estimate the rotation between two point clouds. This observation is illustrated in Fig. 1 (a), where the rotation aligning the two corresponding 3D local patches is exactly the ground truth rotation for the registration of two point clouds. Based on this observation, a pair of matched descriptors, called rotation-equivariant descriptors, will have the ability to estimate a rotation if they encode such orientation information of the 3D local patches. Only few existing registration works [19, 22] are based on the rotation-equivariant descriptors. These methods rely on the fragile LRF as the orientation [22] or directly regress a rotation from an unaligned patch pair [19], which does not generalize well to unseen point pairs.

In this paper, we aim at designing a novel descriptor-based framework for point cloud registration, which simultaneously utilizes the rotation-invariance to find matches and the rotation-equivariance to find plausible rotations. Instead of relying on a vulnerable external LRF, the rotation invariance is naturally achieved by feature extraction on the $SO(3)$ space via neural networks [10, 13, 26, 41], which takes advantage of powerful ability of neural networks to achieve robustness to noise and density variation of point clouds. Meanwhile, by utilizing the rotation equivariance, we can estimate the rotation from just one matched point pair. By combining the estimated rotation with the translation from the same matched point pair, we are able to use only one match pair as a hypothesis in RANSAC to estimate the global transformation. In light of this, we call our framework *You Only Hypothesize Once* (YOHO), which greatly improves both the accuracy and efficiency of registration by reducing the searching space for transformations.

Specifically, our descriptor, called YOHO-Desc, is built on a so-called group feature defined on the icosahedral group G , the largest

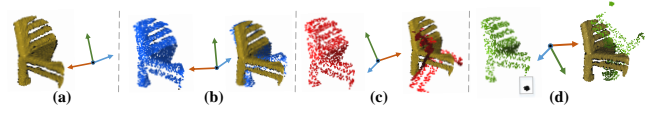


Figure 2: LRF construction by PCA is sensitive to density variation or noise. (a) Original patch and its LRF. We Randomly downsample the point number to 2048 (b) and 1024 (c) and we add a small set of noise points (black) in (d), all of which lead to a obvious change of the LRF.

finite subgroup of $SO(3)$, with $f : G \rightarrow \mathbb{R}^n$. An essential observation on this group feature is that rotating the input point cloud with any rotations $g \in G$ will produce a new group feature f' which is only a permuted version of the original one: $f'(h) = f(gh)$, where $h \in G$. Three technical merits can be achieved. 1) **Rotation estimation**. A relative rotation can be computed by finding a permutation in G that aligns two group features. 2) **Rotation invariance**. The permutation can be simply eliminated by applying a pooling operator on the group feature, which results in a rotation-invariant descriptor. 3) **Discriminative**. By applying a group-based convolution operator on the group feature f , the descriptor is able to exploit discriminative patterns defined on the group G . To this end, modified RANSAC algorithms are designed to utilize both the estimated matches and the estimated rotations for accurate and efficient alignments.

We evaluate the performance of YOHO on the widely-used benchmarks 3DMatch [81] dataset, the 3DLoMatch [34] dataset, the ETH [31] dataset and the WHU-TLS [21] dataset. The results show that YOHO achieves better or comparable accuracy of registration than the state-of-the-arts even with only 1000 RANSAC iterations, while existing methods commonly need 50000 iterations. The reduced RANSAC iterations greatly save time to reconstruct a completed point cloud from partial scans.

Our contributions are summarized as follows:

- (1) We propose a novel rotation-equivariant local descriptor for point cloud registration, which is built on the icosahedral group features and general to combine with fully convolutional or patch-based backbones for promising enhancements.
- (2) We utilize the rotation-equivariance of the descriptor for the rotation estimation which greatly reduces the searching space for true transformations.
- (3) We design a registration framework YOHO, which achieves superior performance on benchmarks with less than 1k RANSAC iterations.

2 RELATED WORK

2.1 Point cloud registration

Feature-based methods. Using local descriptors for point cloud registration has a long history [20, 21, 33]. Traditional methods [1, 22, 32, 37, 62, 63] use handcrafted features to construct descriptors. After the prosperity of deep learning models, learning based descriptors [7, 12, 17, 31, 35, 43, 48] achieve impressive improvements over traditional handcrafted descriptors. Most of these methods achieve rotation invariance by PCA on the neighborhood to find one axis [3, 52], i.e. normal, or three axes directly [7, 31, 67]. Some other works [17, 18] handcraft some rotation-invariant features

and then use a network to extract descriptors from these invariant features. However, the PCA on the neighborhood is not robust to noise or density variations and handcrafted invariant features usually lose lots of information.

Recent works [10, 51] resort to group convolution layers [13] and pooling on the group to extract rotation-invariant descriptors for point cloud registration. The most similar one is EPN [10], which also adopts icosahedral group convolution for point cloud registration. The key difference is that YOHO proposes to utilize the estimated rotation in the modified RANSAC for fast and accurate partial scan alignment while EPN does not consider such rotations in the RANSAC, which leads to less efficient and less accurate results as demonstrated in experiments. We provide more discussion about EPN and YOHO in appendices.

There are only few existing works [19, 22, 88] estimate a rotation from a single descriptor pair for point cloud registration. The most relevant work is RelativeNet [19] which direct regress a rotation from a descriptor pair. However, such regression does not generalize well to unseen data in training set as shown by experiments. In contrast, by utilizing feature map defined on the icosahedral group, YOHO is able to estimate a plausible rotation by finding a permutation to align two feature maps, which improves the generalization ability of YOHO-Desc to unseen data. Meanwhile, YOHO-Desc achieves both rotation invariance and equivariance in a compact framework while RelativeNet relies on a separated PPF-FoldNet [17] to construct rotation-invariant descriptors.

Direct registration methods. Instead of feature extraction on two point clouds separately, some other works find the alignment by simultaneously considering information from both two point clouds [5, 9, 61, 76]. These works either directly solve for the transformation parameters by networks [4, 36, 44, 79, 86] or estimate more accurate correspondences by conditioning descriptors of one point cloud on the other point cloud [6, 11, 27, 34, 42, 49, 55, 60, 69, 70, 77]. In general, more accurate correspondences can be found due to additional information from the other point cloud. However, YOHO does not belong to this category because YOHO-Desc is constructed separately in two point clouds and the correspondences are established simply by the nearest neighbor matching.

2.2 Equivariant feature learning

Recent works [13–16, 23–25, 57, 73] develop tools to learn equivariant features. Some works [10, 26, 38, 41, 58, 64, 66, 78, 84] design architectures to learn a rotation-equivariant or -invariant features on point clouds. Recent Neural Descriptor Field [65] applies equivariance [16] to learn category-level descriptors with self-supervision. YOHO focuses on applying these rotation-equivariant feature learning techniques for the general point cloud registration task. The most similar works are [10, 26, 41]. These works mainly focus on the rotation-invariance for point cloud recognition or shape description. In comparison, YOHO simultaneously takes advantage of both the rotation equivariance and the rotation invariance for robust and effective point cloud registration.

3 METHOD

Overview. Given two unaligned point clouds \mathcal{P} and \mathcal{Q} , our target is to find a transformation $T = \{R, t\} \in SE(3)$ that can integrate

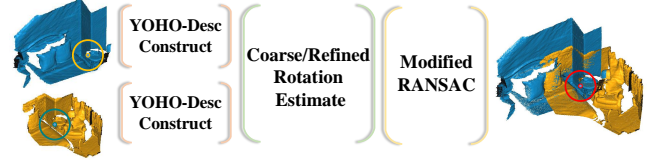


Figure 3: Overview of YOHO. YOHO-Desc is constructed on point cloud separately and is matched to build correspondences. On every correspondence, a coarse rotation and a refined rotation are estimated, which are further utilized by modified RANSAC algorithms to find correct transformations.

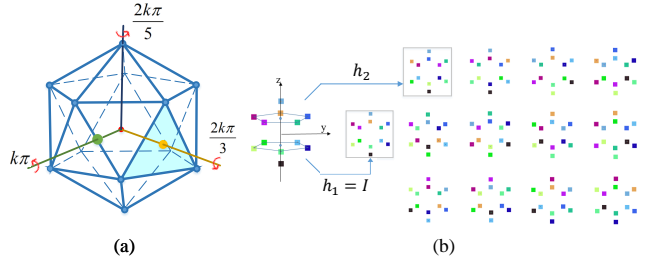


Figure 4: (a) Icosahedral group contains $k\pi$ rotations around axes through edge centers or $2k\pi/3$ rotations around axes through face centers or $2k\pi/5$ rotations around axes through vertices. (b) The neighborhood set H . Different colors are drawn on the vertices of an icosahedron. H contains the identity element and 12 rotations that permute the identity vertices to the right 12 vertices. Note all 12 rotations are 72° rotations about axes.

them into a whole point cloud. The whole pipeline of YOHO is shown as Fig. 3. In the following, we first introduce the background in Sec. 3.1. Then, we introduce how to extract YOHO-Desc on a point cloud in Sec. 3.2. The extracted YOHO-Desc will be matched to produce correspondences and we introduce how to estimate a rotation on a correspondence via YOHO-Desc in Sec. 3.3. Finally, we utilize the estimated rotations in two modified RANSAC algorithms to find the transformations in Sec. 3.4.

3.1 Preliminary

In this section, we only introduce some backgrounds about $SO(3)$ space and recommend readers refer to [13, 26, 47].

Icosahedral group. We define feature maps on the largest discrete finite subgroup of $SO(3)$, i.e. icosahedral group G . The icosahedral group consists of 60 rotations that keep a regular icosahedron invariant, as shown in Fig. 4. Due to the closure of a group, $\forall g \in G$ and $\forall h \in G$, we have $gh \in G$, where gh means the composition of the rotation g and the rotation h to get a new rotation.

Group action. We can use an element $g \in G$ to act on other objects. Two kinds of group actions are used: $T_g \circ \mathcal{P}$ means rotating a set of points \mathcal{P} by the rotation $g \in G$ and $P_g \circ f$ means permuting the matrix f according to $g \in G$, which we will give a more detailed description in Sec. 3.2.

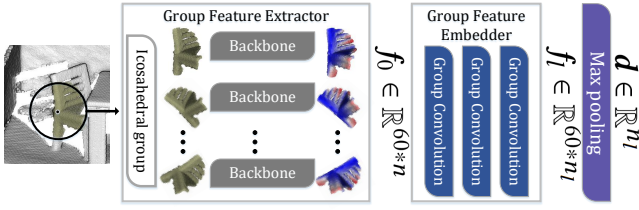


Figure 5: Pipeline for the descriptor construction.

Neighborhood set. In order to define the convolution layer on the icosahedral group G , we define a neighborhood set H as shown in Fig. 4, which is similar to the 3×3 or 5×5 neighborhood in the vanilla image convolution.

3.2 Descriptor construction

For a point $p \in \mathcal{P}$, we construct a YOHO-Desc from its local 3D patch $N_p = \{p_i | \|p_i - p\| < r\}$, by two modules called Group Feature Extractor and Group Feature Embedder, as shown in Fig. 5.

Group feature extractor. Given the input neighborhood point set N_p , we rotate it with an element g in the icosahedral group G . Every rotated point set is processed by the same point set feature extractor called *backbone* to extract a n -dimensional feature, which can be expressed by

$$f_0(g) = \phi(T_g \circ N_p), \quad (1)$$

where $f_0 : G \rightarrow \mathbb{R}^{n_0}$ is the output group feature for the point p , ϕ is the backbone and $T_g \circ N_p$ means rotating the point set N_p with the rotation g . Since the icosahedral group G has 60 rotations, the output group feature f_0 is actually stored by a $60 \times n_0$ matrix where the row index stands for different rotations in G . Note any point set feature extractor, including PointNet [59] and fully convolutional extractor FCGF [12] or D3Feats [7], can be used as the backbone. When using the lightweight fully convolution based extractor as the backbone, we directly rotate the whole point cloud and the neighborhood set is implicitly defined by convolution operators.

Group feature embedder. The group feature can be processed by a localized icosahedral group convolution [26] as follows,

$$[f_{k+1}(g)]_j = \sum_i^{13} w_{j,i}^T f_k(h_i g) + b_j, \quad (2)$$

where k is the index of the layers, $f_k(g) \in \mathbb{R}^{n_k}$ and $f_{k+1}(g) \in \mathbb{R}^{n_{k+1}}$ are the input and output feature respectively, $[\cdot]_j$ means the j -th element from the vector, $h_i \in H$ are all elements from the neighborhood set H , $w_{j,i} \in \mathbb{R}^{n_k}$ is a trainable n_k -dimensional weight defined on the h_i and b_j is a trainable bias term. Note that the $j = 1, \dots, n_{k+1}$ is the index for the output feature dimension and the composition $h_i g$ is also an element in G due to the closure property. Such a group convolution layer enables us to exploit the local patterns defined on the icosahedral group. To this end, l group convolution layers defined in Eq. 2 along with subsequent ReLU and Batch Normalization layers are stacked to construct the group feature embedder.

Rotation equivariance. An important property on the group feature f_k is that using a rotation $h \in G$ to rotate the input point set

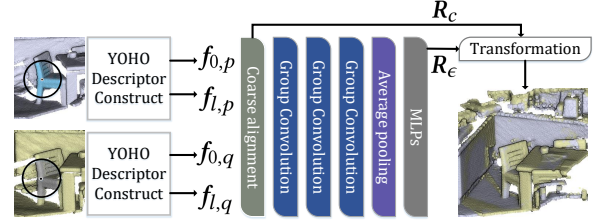


Figure 6: Pipeline for the rotation estimation.

N_p will only result in a permuted version f'_k of the original group feature f_k , which is

$$f'_k = P_h \circ f_k, \quad (3)$$

where both f'_k and f_k are group features represented by $60 \times n_k$ matrices and $P_h \circ f_k$ is actually a permutation of row vectors of the matrix f_k brought by h . Note Eq. 3 holds for all group features $k = 0, 1, \dots, l$. We leave the proof of Eq. 3 in the appendices.

Invariant descriptor. Based on the equivariance property, we can construct a rotation-invariant descriptor from the final layer group feature f_l by simply applying an average-pooling operator on all group elements, which is,

$$d = \text{AvgPool}(f_l). \quad (4)$$

The resulted descriptor d is invariant to all rotations in the icosahedral group, which can be easily verified that $d' = \text{AvgPool}(P_h \circ f_l) = \text{AvgPool}(f_l) = d$ since AvgPool is unaffected by permutations. Though d is not strictly invariant to rotations outside the icosahedral group, the existing rotation invariance already provides a strong inductive bias for the network to learn invariance to other rotations.

3.3 Rotation estimation

We apply a nearest neighborhood (NN) matcher on the descriptors d with a mutual nearest check [3, 34, 81] from two scans to find a set of putative correspondences. In this section, we introduce how to compute a rotation on every correspondence.

Coarse rotations. Given two matched points p and q along with their YOHO-Desc, we find a coarse rotation R_c by aligning two group features with a permutation

$$R_c = \underset{g \in G}{\text{argmin}} \|f_{l,q} - P_g \circ f_{l,p}\|_2, \quad (5)$$

where $f_{l,p}$ is the final group feature for the point p and we iterate all 60 permutations in $\{P_g | g \in G\}$ to find the best one that minimizes the L2 distance between group features.

Refined rotations. Since the group G is a discretization of $SO(3)$, we cannot directly get a precise rotation by finding the best permutation. To find such a precise rotation, we use a regressor to compute the residual between the coarse rotation and the true rotation by

$$R_e = \eta([f_{0,q}; f_{l,q}; P_{R_c} \circ f_{0,p}; P_{R_c} \circ f_{l,p}]), \quad (6)$$

where R_e is the rotation residual, $[\cdot; \cdot]$ means the concatenation of features along the channel direction, $P_{R_c} \circ f$ means the permutation of f by R_c , the resulted feature map by the concatenation is still a group feature with size $60 \times (2n_0 + 2n_l)$ and the η is a network. Note both the final group feature f_l and the initial group feature f_0

are fed to the network η . η is called Rotation Residual Regressor, which applies group convolutions defined by Eq. 2 on the input group feature. After being processed by the group convolutions, the group feature is average-pooled to a single feature vector which is further processed by a Multi-Layer Perceptron (MLP) to regress a rotation residual in the quaternion form. The whole network is shown in Fig. 6. The rotation residual R_ϵ is composited with the coarse rotation R_c to produce the refined rotation $R_r = R_\epsilon R_c$.

3.4 Modified RANSAC algorithms

YOHO descriptors are extracted separately on two point clouds (Sec. 3.2) and are matched by a NN matcher to produce a set of correspondences $C = \{c_i = (\mathbf{p}_i, \mathbf{q}_i) | \mathbf{p}_i \in \mathcal{P}, \mathbf{q}_i \in \mathcal{Q}\}$. On every correspondence c_i , a coarse rotation $R_{c,i}$ and a refined rotation $R_{r,i}$ are computed as stated in Sec. 3.3. In a standard RANSAC algorithm, a correspondence triplet is randomly selected to compute a transformation T and the transformation with the largest number of inliers will be selected as the output transformation. In our case, we propose two different ways, called Coarse Rotation Verification (CRV) and One-Shot Transformation Estimation (OSE), to incorporate the estimated rotations in the RANSAC pipeline, which greatly reduces the searching space for transformations.

Coarse rotation verification. Instead of randomly selecting all correspondence triplets to compute T , we limit feasible correspondence triplets to $\{(i, j, k) | R_{c,i} = R_{c,j} = R_{c,k}\}$ that have the same estimated coarse rotations. Such a verification greatly reduces the searching space to find an accurate transformation.

One-shot transformation estimation. Given a correspondence c_i and its refined rotation $R_{r,i}$, we can compute the transformation T directly by $R = R_{r,i}$ and $\mathbf{t} = \mathbf{q}_i - R\mathbf{p}_i$. Given n correspondences, we will only have n feasible transformation hypotheses which are much less than the $n \times (n-1) \times (n-2)/6$ feasible triplets in the original RANSAC. Moreover, if the inlier ratio in the putative correspondences is α , then we will have a chance of α to find the true transformation while in the original RANSAC, such chance is α^3 .

3.5 Implementation details

By default, we implement YOHO using FCGF [12] as the backbone. In the appendices, we also provide results with PointNet [59] as the backbone to show YOHO's ability to work with different backbones. The group convolution network in the group feature embedding has 4 group convolution layers. The final descriptor \mathbf{d} and the group feature \mathbf{f}_l used before coarse rotation estimation are all normalized by their L2 norms. The rotation residual regressor has 3 group convolution layers and 3 layers in the MLP after the average-pooling layer. A more detailed implementation about the network architecture can be found in our project page. To build the putative correspondences, YOHO-Desc are matched by a nearest neighborhood matcher with a mutual nearest test, which is exactly the same as used in [31].

Loss for descriptor construction. Given a batch of ground-truth point pairs $\{(\mathbf{p}, \mathbf{p}^+)\}$ as well as their ground-truth rotations $\{R_p\}$, we compute the outputs of group feature embedder, which are the rotation invariant descriptors $\{(\mathbf{d}_p, \mathbf{d}_p^+)\}$, the rotation equivariant group features $\{(\mathbf{f}_p, \mathbf{f}_p^+)\}$, and the corresponding ground truth coarse rotations $\{g_p^+\}$. For every sample in the batch, we compute

the loss:

$$\ell_1(\mathbf{d}, \mathbf{d}^+, D^-) = \frac{e^{\|\mathbf{d}-\mathbf{d}^+\|_2} - \min_{\mathbf{d}^- \in D^-} e^{\|\mathbf{d}-\mathbf{d}^-\|_2}}{e^{\|\mathbf{d}-\mathbf{d}^+\|_2} + \sum_{\mathbf{d}^- \in D^-} e^{\|\mathbf{d}-\mathbf{d}^-\|_2}} \quad (7)$$

$$\ell_2(\mathbf{f}, \mathbf{f}^+, g^+) = -\log\left(\frac{e^{\langle \mathbf{f}, \mathbf{f}_p^+ \circ \mathbf{f}^+ \rangle}}{\sum_{g \in G} e^{\langle \mathbf{f}, \mathbf{f}_p^+ \circ g \rangle}}\right) \quad (8)$$

$$\ell_d = \lambda * \ell_1(\mathbf{d}, \mathbf{d}^+, D^-) + \ell_2(\mathbf{f}, \mathbf{f}^+, g^+), \quad (9)$$

where the subscript \mathbf{p} is omitted for simplicity. Eq. 7 is used for the supervision of the rotation invariant descriptor, \mathbf{d} is a rotation invariant descriptor, \mathbf{d}^+ is its matched descriptor, D^- are the other negative descriptors in the batch and $\|\cdot\|_2$ is the L2 norm. Eq. 8 is used for the supervision of the coarse rotation estimation. \mathbf{f} is a flattened query group feature vector, $\langle \cdot, \cdot \rangle$ is the vector dot product and g^+ is the ground truth coarse rotation between \mathbf{f} and \mathbf{f}^+ . λ is set to 5. ℓ_1 is the batch-hard loss while ℓ_2 encourage the alignments of two group features under the ground-truth rotations. The reason to use ℓ_2 is that though the equivariance property is theoretically guaranteed, some noise or density variations may break the equivariance so that supervision from ℓ_2 will make the network more robust to these factors.

Loss for Rotation Residual Regressor. Given a ground-truth point pair $(\mathbf{p}, \mathbf{p}^+)$ in the batch and its ground-truth rotation R_p . We extract the group features using the group feature extractor and embedder. Then, we coarsely align the group features using the ground truth coarse rotation g_p^+ . Finally, we estimate its residual rotation $R_{\epsilon,p}$ using the Rotation Residual Regressor and supervise the Regressor by:

$$\ell_R(\mathbf{p}, \mathbf{p}^+) = \|R_{\epsilon,p} - R_{\epsilon,p}^+\|_2 \quad (10)$$

where $R_{\epsilon,p}^+ = R_p g_p^{+T}$ is the ground truth residual rotation. $R_{\epsilon,p}$, $R_{\epsilon,p}^+$ are represented in the quaternion form.

4 EXPERIMENTS

In the following, we evaluate two YOHO models for point cloud registration, which are the YOHO using coarse rotation verification (YOHO-C) and the YOHO with the one-shot transformation estimation (YOHO-O).

4.1 Experimental protocol

Datasets. We follow exactly the same experiment protocol as [81] to prepare the training and testing data on the indoor 3DMatch dataset. In this setting, 5000 predefined keypoints are extracted on every scan. However, since the original testset on 3DMatch only contains scan pairs with $>30\%$ overlap, we also evaluate the model on the 3DLoMatch dataset [34] with overlap between 10% and 30% to demonstrate our robustness to low overlap. We also evaluate the proposed method on the outdoor ETH dataset [31] and the outdoor WHU dataset [21], which contain more point density variations than the 3DMatch. Note that our model is trained on the 3DMatch dataset and is solely evaluated on the ETH dataset, the WHU-TLS dataset and the 3DLoMatch dataset. For the FCGF backbone, the downsampled voxel size is 2.5cm, 15cm and 0.8m for the 3DMatch, ETH and WHU-TLS datasets according to their scales.

Metrics. Feature Matching Recall (FMR) [12, 31, 34], Inlier Ratio (IR) [34] and Registration Recall (RR) [7, 12, 34] are used as metrics for evaluations. A correspondence is regarded as a correct one if the distance between its two matched points is $\leq \tau_c$ under the ground truth transformation. FMR is the percentage of scan pairs with correct correspondence proportions more than 5% found by the local descriptor, same as used in [3, 34]. IR is the average correct correspondence proportions. RR is the percentage of correctly aligned scan pairs, which means that the average distance between the points under the estimated transformation and these points under the ground truth transformation is less than τ_r . For RR, we follow [34] and report the number of RANSAC iterations to achieve the performance. Due to the randomness of RANSAC, we run YOHO three times to compute the mean of RR on all datasets.

Baselines. We mainly compare YOHO with state-of-the-art learning based descriptors: PerfectMatch [31], FCGF [12], D3Feat [7], LMVD [43], EPN [10] SpinNet [3], and a learning-based matcher: Predator [34]. On the 3DMatch dataset, we also include the results from RelativeNet [19] which also learns rotation equivariance for registration. For all baseline methods, we report the results in their papers or evaluate with their official codes or models. For a fair comparison, baseline methods uses the RANSAC implementation in Open3D [87] with engineering optimization like concurrent computation, optimized hyperparameters and distance checks.

4.2 Results on 3DMatch/3DLoMatch

Results of YOHO and baseline models on the 3DMatch dataset and the 3DLoMatch dataset are shown in Table 1. Some qualitative results are shown in Fig. 7. With 50 times fewer RANSAC iterations, YOHO still outperforms all baseline methods. The improvements on RR of YOHO mainly come from YOHO’s utilization of rotation equivariance, which greatly reduces the searching space.

4.3 Results on the ETH dataset

In Table 2, we provide results in two different thresholds for correspondences and registration and some qualitative results are shown in Fig. 7. In the strict setting with $\tau_c = 0.1m$ and $\tau_r = 0.2m$, YOHO underperforms SpinNet. The reason is that the FCGF backbone of YOHO downsamples input point clouds with a voxel size of 0.15m, which limits the accuracy of correspondences found by YOHO. SpinNet extracts local descriptors on every point independently, which has better accuracy but at a noticeable cost of longer computation time (62.6 min) than YOHO (4.6 min). In a slightly loose setting with $\tau_c = 0.2m$ and $\tau_r = 0.5m$, YOHO outperforms SpinNet in terms of IR and RR.

Though the downsampled voxel size in FCGF makes YOHO unable to produce very accurate matches, we show that this can be easily improved by a commonly-used ICP [5] post-processing. In Table 3, we show RR using ICP post-processing, in which YOHO-C+ICP outperforms SpinNet+ICP in all thresholds including the strictest one with $\tau_r = 0.05m$. Additional results on the WHU-TLS dataset can be found in the appendices.

4.4 Ablation studies

To show the effectiveness of each component in YOHO, we conduct ablation studies on the 3DMatch dataset. The results are shown

	3DMatch		3DLoMatch	
	Origin	Rotated	Origin	Rotated
Feature Matching Recall (%)				
RelativeNet[19]	74.6	-	-	-
PerfectMatch[31]	95.0	94.9	63.6	63.4
FCGF[12]	97.4	97.6	76.6	75.4
D3Feat[7]	95.6	95.5	67.3	67.6
LMVD[43]	97.5	96.9	<u>78.7</u>	<u>78.4</u>
EPN[10]	<u>97.6</u>	<u>97.6</u>	76.3	76.6
SpinNet[3]	<u>97.6</u>	97.5	75.3	75.3
Predator[34]	96.6	96.7	78.6	75.7
YOHO	98.2	98.1	79.4	79.2
Inlier Ratio (%)				
PerfectMatch[31]	36.0	35.8	11.4	11.7
FCGF[12]	56.8	56.2	21.4	21.6
D3Feat[7]	39.0	39.2	13.2	13.5
LMVD[43]	45.1	45.0	17.3	17.0
EPN[10]	49.5	48.6	20.7	20.6
SpinNet[3]	47.5	47.2	20.5	20.1
Predator[34]	<u>58.0</u>	<u>58.2</u>	<u>26.7</u>	<u>26.2</u>
YOHO	64.4	65.1	25.9	26.4
	#Iters	Registration Recall (%)		
RelativeNet[19]	~1k	77.7	-	-
PerfectMatch[31]	50k	78.4	78.4	33.0
FCGF[12]	50k	85.1	84.8	40.1
D3Feat[7]	50k	81.6	83.0	37.2
LMVD[43]	50k	82.5	82.2	41.3
EPN[10]	50k	88.2	87.6	58.1
SpinNet[3]	50k	88.6	88.4	59.8
Predator[34]	50k	89.0	88.4	59.8
YOHO-C	0.1k	90.1	89.4	62.9
	1k	<u>90.5</u>	<u>90.6</u>	<u>64.9</u>
YOHO-O	0.1k	90.3	90.2	64.8
	1k	90.8	90.6	65.2

Table 1: Results on the 3DMatch and 3DLoMatch datasets. The rotated version means that we adding additional arbitrary rotations to all point clouds. Same as [3, 34], we set $\tau_c=0.1m$ and $\tau_r=0.2m$ to compute metrics.

	T(min)	$\tau_c = 0.1m, \tau_r = 0.2m$			$\tau_c = 0.2m, \tau_r = 0.5m$		
		FMR	IR	RR	FMR	IR	RR
PerfectMatch[31]	53.7	<u>79.2</u>	<u>13.3</u>	83.5	<u>96.8</u>	19.7	86.4
FCGF[12]	5.2	47.3	5.5	48.2	59.0	16.7	52.2
D3Feat[7]	4.1	59.1	7.9	55.2	63.3	18.2	59.1
SpinNet[3]	62.6	92.0	14.3	93.4	99.4	<u>23.2</u>	<u>96.0</u>
Predator[34]	16.7	25.4	3.7	52.3	65.6	11.1	74.7
YOHO-C	<u>4.6</u>	71.1	10.6	<u>87.1</u>	<u>96.8</u>	26.8	96.8
YOHO-O	6.2	71.1	10.6	74.1	<u>96.8</u>	26.8	94.7

Table 2: Results on the ETH dataset. RANSAC is executed 1k iterations for YOHO and 50k for other methods. T is the total time for the registration on the ETH dataset.

in Table 4. We design 5 models sequentially and every model only differs from the previous model on one component.

Invariance via group features. The model 0 in Table 4 simply applies FCGF [12] to construct descriptors. Based on the model 0,

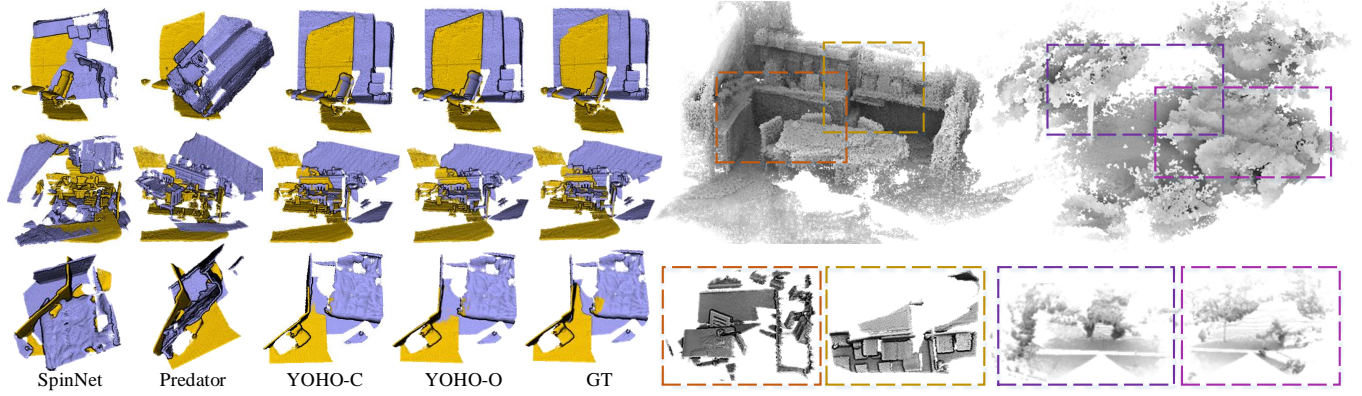


Figure 7: (Left) Qualitative comparison with baselines. (Right) Completed scenes by YOHO and some input partial scans.

	T(min)	$\tau_r(m)$						
		0.05	0.1	0.15	0.2	0.25	0.3	0.5
SpinNet[3]+ICP	66.8	92.1	96.4	96.2	96.7	96.7	96.8	96.8
YOHO-C+ICP	9.1	92.3	97.0	97.5	97.5	97.5	97.6	97.8
YOHO-O+ICP	11.2	89.5	94.1	94.7	94.9	95.1	95.4	95.9

Table 3: RR on the ETH dataset with ICP. T is the total time for the registration, including the time used in ICP.

The model 1 achieves rotation invariance by constructing the icosahedral group features with the same FCGF and average-pooling on the group features. By comparing the model 1 with the model 0, we can see that achieving rotation invariance from group features is more robust. Further analysis on robustness against noise and density variations can be found in the appendices.

Coarse rotation verification. Based on the model 1, the model 2 estimates the coarse rotation from the group features f_0 and uses the coarse rotation verification (CRV) in the RANSAC. By comparing the model 2 with the model 1, CRV achieves higher RR than the vanilla RANSAC with 50 times fewer iterations.

Group convolution layer. Based on the model 2, the model 3 adds the proposed group convolutions before average-pooling, i.e. YOHO-C. The group convolution enables the network to exploit patterns defined on the icosahedral group, which brings about 4.9% improvements on the FMR and 9.6% improvements on the RR.

One-shot transformation estimation. Based on the model 3, the model 4 estimates the rotation residuals and uses the refined rotations to do the one-shot transformation estimation (OSE) in RANSAC, i.e. YOHO-O, which brings further improvements on RR.

4.5 Analysis

We provide more comparisons, analysis on iteration number and running time in the following. More analysis about robustness to noise, point density can be found in the appendices.

Performance with different numbers of sampled points. Results in Table 5 show that YOHO consistently outperforms all other local descriptors in all cases but underperforms the learning-based matcher Predator [34] when very few keypoints are used. The reason is that as a matcher, Predator is able to simultaneously utilize information from both source and target point clouds to find overlapped regions. However, YOHO only extracts descriptors

id	Inv.	GConv.	#Iter	RANSAC	FMR	RR
0	None		50k	Vanilla	90.0	76.2
1	Group		50k	Vanilla	93.3	77.8
2	Group		1k	CRV	93.3	80.9
3	Group	✓	1k	CRV	98.2	90.5
4	Group	✓	1k	OSE	98.2	90.8

Table 4: Ablation studies on the 3DMatch dataset. The “Inv.” means how to get rotation invariance. “None” means no rotation invariance while “Group” means average-pooling on icosahedral group features. “GConv” means the proposed group convolution. “CRV” means coarse rotation verification while “OSE” means one-shot rotation estimation.

on every point cloud separately, which is oblivious of the other point cloud to be aligned. Meanwhile, it is possible to incorporate YOHO within a learning-based matcher like Predator [34] for better performance, which we leave for future works.

Necessary iteration number. To further show how many iterations are necessary to find a correct transformation, we further conduct an experiment on the 3DMatch/3DLoMatch datasets. For every scan pair, we count the number of iterations required to find a correct transformation. As shown in Fig. 8, a point (R,N) in the figure means R% scan pairs use less than N iterations to find the true transformation. The iteration ends once a true transformation is found while RANSAC chooses the transformation with a max inlier number. Thus, the curve only reveals correspondence quality but is not affected by the termination criteria of RANSAC.

The results show that both YOHO-C and YOHO-O find true transformations very fast with less than 400 iterations. In comparison, all baseline methods only find a small portion of true transformations within 500 iterations, even though they can also achieve good RRs after 50k iterations as shown in Table 1. Moreover, an even more significant performance gap is shown on the 3DLoMatch dataset. The reason is that the smaller overlap brings a lower inlier ratio on the putative correspondences, which is less than 0.1 in general. In this case, selecting a triplet of inliers in baseline methods will have a probability less than $0.1^3 = 0.001$ while the probability of finding true transformations in YOHO-O is the same as the inlier ratio because it only needs one matched pair to compute a transformation.

Running time. On a desktop with an i7-10700 CPU and a 2080Ti GPU, the time consumption is listed in Table 6. We provide the time

#Samples	3DMatch					3DLoMatch				
	5000	2500	1000	500	250	5000	2500	1000	500	250
Feature Matching Recall (%)										
FCGF[12]	97.4	97.3	97.0	96.7	96.6	76.6	75.4	74.2	71.7	67.3
D3feat[7]	95.6	95.4	94.5	94.1	93.1	67.3	66.7	67.0	66.7	66.5
SpinNet[3]	97.6	97.2	96.8	95.5	94.3	75.3	74.9	72.5	70.0	63.6
Predator[34]	96.6	96.6	96.5	96.3	96.5	78.6	77.4	76.3	75.7	75.3
YOHO	98.2	97.6	97.5	97.7	96.0	79.4	78.1	76.3	73.8	69.1
Inlier Ratio (%)										
FCGF[12]	56.8	54.1	48.7	42.5	34.1	21.4	20.0	17.2	14.8	11.6
D3feat[7]	39.0	38.8	40.4	41.5	41.8	13.2	13.1	14.0	14.6	15.0
SpinNet[3]	47.5	44.7	39.4	33.9	27.6	20.5	19.0	16.3	13.8	11.1
Predator[34]	58.0	58.4	57.1	54.1	49.3	26.7	28.1	28.3	27.5	25.8
YOHO	64.4	60.7	55.7	46.4	41.2	25.9	23.3	22.6	18.2	15.0
Registration Recall (%)										
FCGF[12]	85.1	84.7	83.3	81.6	71.4	40.1	41.7	38.2	35.4	26.8
D3feat[7]	81.6	84.5	83.4	82.4	77.9	37.2	42.7	46.9	43.8	39.1
SpinNet[3]	88.6	86.6	85.5	83.5	70.2	59.8	54.9	48.3	39.8	26.8
Predator[34]	89.0	89.9	90.6	88.5	86.6	59.8	61.2	62.4	60.8	58.1
YOHO-C	90.5	89.7	88.4	87.6	82.8	64.9	65.1	61.4	54.5	43.9
YOHO-O	90.8	90.3	89.1	88.6	84.5	65.2	65.5	63.2	56.5	48.0

Table 5: Quantitative results on the 3DMatch and the 3DLoMatch datasets using different numbers of sampled points. RANSAC is executed 1k iterations for YOHO and 50k for other methods.

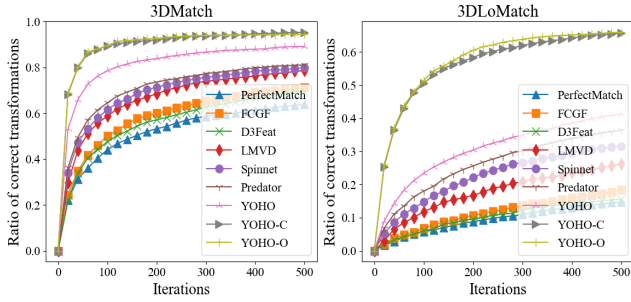


Figure 8: Ratio of correct transformations versus iteration number on the 3DMatch dataset and the 3DLoMatch dataset.

t_1 used in the feature extraction of one point cloud fragment and the time t_2 used in aligning a point cloud pair by RANSAC, and the total time cost T on registration of the 3DMatch and the 3DLoMatch dataset. The feature extraction in YOHO costs longer time than baselines because it needs to compute the backbone network 60 times. However, since these 60 point clouds are all rotated versions of the original one, they share many common computations like neighborhood querying for speeding up. Aligning scan pairs with RANSAC in YOHO is much faster than baselines. Meanwhile, the baselines uses advanced RANSAC implementation with engineering optimization, so YOHO with 1k iterations is not strictly 50 times faster than baselines with 50k iterations. In total, YOHO still takes the shortest time because there are 433 partial scans, 1623 scan pairs in 3DMatch and 1781 pairs in 3DLoMatch and we only need to extract features once and use them in all subsequent pair alignments.

Method	#Iters	t_1 (s/pc)	t_2 (s/pcp)	T (min)
PerfectMatch[31]	50k	22.125	0.368	180.547
FCGF[12]	50k	0.381	0.384	24.535
D3Feat[7]	50k	0.122	0.351	20.794
EPN[10]	50k	342.246	0.437	2494.668
SpinNet[3]	50k	26.556	0.413	215.077
Predator[34]	50k	-	1.221	69.271
YOHO-C	1k	1.812	0.056	16.253
YOHO-O	1k	1.812	0.167	22.553

Table 6: The time consumption for the registration on the 3DMatch dataset and the 3DLoMatch dataset. We provide the time t_1 used in the feature extraction of one point cloud fragment and the time t_2 in aligning a point cloud pair, and the total time T on the registration of the 3DMatch and the 3DLoMatch dataset.

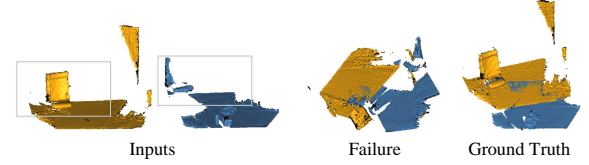


Figure 9: A failure case on the 3DLoMatch dataset. The overlap area is planar, leading to ambiguity in rotation estimation.

Limitations. The limitation of our methods mainly lies in two fronts: 1) When the overlap region of two scans mainly consists of planar points, YOHO may fail to find the correct rotations since rotation estimation is ambiguous on planar points as in Fig. 9. 2) Though YOHO is overall computation-efficient due to the improvement in RANSAC, the construction of YOHO-Desc is less efficient due to 60 times forward passes of backbone. This may possibly be optimized by group simplification [26], limiting rotations to $SO(2)$, or advanced equivariance learning techniques [16, 68], which we leave for future works.

5 CONCLUSION

In this paper, we propose a framework called YOHO for point cloud registration of two partial scans. The key of YOHO is a descriptor that simultaneously has rotation invariance and rotation equivariance. The descriptor is constructed by using the features defined on the icosahedral group which is rotation-equivariant by itself and can be pooled to achieve rotation invariance. We utilize the rotation-invariant part of YOHO-Desc to build correspondences and estimate a rotation per pair with their rotation-equivariant part. The estimated rotations greatly help the subsequent RANSAC to find the correct transformations robustly and accurately. We demonstrate the effectiveness of YOHO in multiple datasets, which achieves state-of-the-art performances with much fewer RANSAC iterations.

6 ACKNOWLEDGEMENT

This research is jointly sponsored by the National Key Research and Development Program of China (No. 2018YFB2100503), the National Natural Science Foundation of China Projects (No. 42172431) and DiDi GAIA Research Collaboration Plan.

REFERENCES

- [1] Dror Aiger, Niloy J Mitra, and Daniel Cohen-Or. 2008. 4-points congruent sets for robust pairwise surface registration. In *SIGGRAPH*. 1–10.
- [2] Aitor Aldoma, Zoltan-Csaba Marton, Federico Tombari, Walter Wohlkinger, Christian Potthast, Bernhard Zeisl, Radu Bogdan Rusu, Suat Gedikli, and Markus Vincze. 2012. Tutorial: Point cloud library: Three-dimensional object recognition and 6 dof pose estimation. *IEEE Robotics & Automation Magazine* 19, 3 (2012), 80–91.
- [3] Sheng Ao, Qingyong Hu, Bo Yang, Andrew Markham, and Yulan Guo. 2021. SpinNet: Learning a General Surface Descriptor for 3D Point Cloud Registration. In *CVPR*.
- [4] Yasuhiro Aoki, Hunter Goforth, Rangaprasad Arun Srivatsan, and Simon Lucey. 2019. PointNetLK: Robust & efficient point cloud registration using pointnet. In *CVPR*.
- [5] K Somani Arun, Thomas S Huang, and Steven D Blostein. 1987. Least-squares fitting of two 3-D point sets. *IEEE Transactions on pattern analysis and machine intelligence* 5 (1987), 698–700.
- [6] Xuyang Bai, Zixin Luo, Lei Zhou, Hongkai Chen, Lei Li, Zeyu Hu, Hongbo Fu, and Chiew-Lan Tai. 2021. PointDSC: Robust Point Cloud Registration using Deep Spatial Consistency. In *CVPR*.
- [7] Xuyang Bai, Zixin Luo, Lei Zhou, Hongbo Fu, Long Quan, and Chiew-Lan Tai. 2020. D3feat: Joint learning of dense detection and description of 3d local features. In *CVPR*.
- [8] Tim Bailey and Hugh Durrant-Whyte. 2006. Simultaneous localization and mapping (SLAM): Part II. *IEEE robotics & automation magazine* 13, 3 (2006), 108–117.
- [9] Sofien Bouaziz, Andrea Tagliasacchi, and Mark Pauly. 2013. Sparse iterative closest point. In *Computer graphics forum*, Vol. 32. Wiley Online Library, 113–123.
- [10] Haiwei Chen, Shichen Liu, Weikai Chen, Hao Li, and Randall Hill. 2021. Equivariant Point Network for 3D Point Cloud Analysis. In *CVPR*.
- [11] Christopher Choy, Wei Dong, and Vladlen Koltun. 2020. Deep Global Registration. In *CVPR*.
- [12] Christopher Choy, Jaesik Park, and Vladlen Koltun. 2019. Fully Convolutional Geometric Features. In *ICCV*.
- [13] Taco Cohen and Max Welling. 2016. Group Equivariant Convolutional Networks. In *ICML*.
- [14] Taco S Cohen, Mario Geiger, Jonas Köhler, and Max Welling. 2018. Spherical CNNs. In *ICLR*.
- [15] Taco S Cohen and Max Welling. 2017. Steerable CNNs. In *ICLR*.
- [16] Congyue Deng, Or Litany, Yueqi Duan, Adrien Poulenard, Andrea Tagliasacchi, and Leonidas Guibas. 2021. Vector Neurons: A General Framework for SO (3)-Equivariant Networks. In *ICCV*.
- [17] Haowen Deng, Tolga Birdal, and Slobodan Ilic. 2018. PPF-FoldNet: Unsupervised learning of rotation invariant 3d local descriptors. In *ECCV*.
- [18] Haowen Deng, Tolga Birdal, and Slobodan Ilic. 2018. PPFNet: Global context aware local features for robust 3d point matching. In *CVPR*.
- [19] Haowen Deng, Tolga Birdal, and Slobodan Ilic. 2019. 3D local features for direct pairwise registration. In *CVPR*.
- [20] Yago Diez, Ferran Roure, Xavier Lladó, and Joaquim Salvi. 2015. A qualitative review on 3D coarse registration methods. *ACM Computing Surveys (CSUR)* 47, 3 (2015), 1–36.
- [21] Zhen Dong, Fuxun Liang, Bisheng Yang, Yusheng Xu, Yufu Zang, Jianping Li, Yuan Wang, Wenxia Dai, Hongchao Fan, Juha Hyypä, et al. 2020. Registration of large-scale terrestrial laser scanner point clouds: A review and benchmark. *ISPRS Journal of Photogrammetry and Remote Sensing* 163 (2020), 327–342.
- [22] Zhen Dong, Bisheng Yang, Yuan Liu, Fuxun Liang, Bijun Li, and Yufu Zang. 2017. A novel Binary Shape Context for 3D local surface description. *ISPRS Journal of Photogrammetry and Remote Sensing* 130 (2017), 431–452.
- [23] Carlos Esteves, Christine Allen-Blanchette, Ameesh Makadia, and Kostas Daniilidis. 2018. Learning SO (3) Equivariant Representations with Spherical CNNs. In *ECCV*.
- [24] Carlos Esteves, Christine Allen-Blanchette, Xiaowei Zhou, and Kostas Daniilidis. 2018. Polar Transformer Networks. In *ICLR*.
- [25] Carlos Esteves, Ameesh Makadia, and Kostas Daniilidis. 2020. Spin-Weighted Spherical CNNs. In *NeurIPS*.
- [26] Carlos Esteves, Yinshuang Xu, Christine Allen-Blanchette, and Kostas Daniilidis. 2019. Equivariant Multi-View Networks. In *ICCV*.
- [27] Kexue Fu, Shaolei Liu, Xiaoyuan Luo, and Manning Wang. 2021. Robust Point Cloud Registration Framework Based on Deep Graph Matching. In *CVPR*.
- [28] Lin Gao, Jie Yang, Tong Wu, Yu-Jie Yuan, Hongbo Fu, Yu-Kun Lai, and Hao Zhang. 2019. SDM-NET: Deep generative network for structured deformable mesh. *ACM Transactions on Graphics (TOG)* 38, 6 (2019), 1–15.
- [29] Qing Hong Gao, Tao Ruan Wan, Wen Tang, and Long Chen. 2019. Object registration in semi-cluttered and partial-occluded scenes for augmented reality. *Multimedia Tools and Applications* 78, 11 (2019), 15079–15099.
- [30] Song Ge and Guoliang Fan. 2015. Non-rigid articulated point set registration for human pose estimation. In *2015 IEEE Winter Conference on Applications of Computer Vision*. IEEE, 94–101.
- [31] Zhan Gojcic, Caifa Zhou, Jan D Wegner, and Andreas Wieser. 2019. The Perfect Match: 3d point cloud matching with smoothed densities. In *CVPR*.
- [32] Yulan Guo, Ferdous A Sohel, Mohammed Bennamoun, Jianwei Wan, and Min Lu. 2013. RoPS: A local feature descriptor for 3D rigid objects based on rotational projection statistics. In *ICCSA*.
- [33] Winston H. Hsu. 2019. Learning from 3D (Point Cloud) Data. In *Proceedings of the 27th ACM International Conference on Multimedia (Nice, France) (MM '19)*. Association for Computing Machinery, New York, NY, USA, 2697–2698. <https://doi.org/10.1145/3343031.3350540>
- [34] Shengyu Huang, Zhan Gojcic, Mikhail Usvyatsov, Andreas Wieser, and Konrad Schindler. 2021. PREDATOR: Registration of 3D Point Clouds with Low Overlap. In *CVPR*.
- [35] Tianxin Huang and Yong Liu. 2019. 3d point cloud geometry compression on deep learning. In *Proceedings of the 27th ACM international conference on multimedia*. 890–898.
- [36] Xiaoshui Huang, Guofeng Mei, and Jian Zhang. 2020. Feature-Metric Registration: A Fast Semi-supervised Approach for Robust Point Cloud Registration without Correspondences. In *CVPR*.
- [37] Seung Hwan Jung, Yeong-Gil Shin, and Minyoung Chung. 2020. Geometric robust descriptor for 3D point cloud. *arXiv preprint arXiv:2012.12215* (2020).
- [38] Seohyun Kim, Jaeyoo Park, and Bohyung Han. 2020. Rotation-Invariant Local-to-Global Representation Learning for 3D Point Cloud. *arXiv preprint arXiv:2010.03318* (2020).
- [39] Junha Lee, Seungwook Kim, Minsu Cho, and Jaesik Park. 2021. Deep Hough Voting for Robust Global Registration. In *Proceedings of the IEEE/CVF International Conference on Computer Vision*. 15994–16003.
- [40] Feiran Li, Kent Fujiwara, Fumio Okura, and Yasuyuki Matsushita. 2021. A Closer Look at Rotation-Invariant Deep Point Cloud Analysis. In *ICCV*.
- [41] Jiaxin Li, Yingcai Bi, and Gim Hee Lee. 2019. Discrete rotation equivariance for point cloud recognition. In *ICRA*.
- [42] Jiahao Li, Changhao Zhang, Ziyao Xu, Hangning Zhou, and Chi Zhang. 2020. Iterative Distance-Aware Similarity Matrix Convolution with Mutual-Supervised Point Elimination for Efficient Point Cloud Registration. In *ECCV*.
- [43] Lei Li, Siyu Zhu, Hongbo Fu, Ping Tan, and Chiew-Lan Tai. 2020. End-to-end learning local multi-view descriptors for 3d point clouds. In *CVPR*.
- [44] Xueqian Li, Jhony Kaesemodel Pontes, and Simon Lucey. 2020. Deterministic PointNetLK for Generalized Registration. *arXiv preprint arXiv:2008.09527* (2020).
- [45] Yang Li and Tatsuya Harada. 2021. Leopard: Learning partial point cloud matching in rigid and deformable scenes. *arXiv preprint arXiv:2111.12591* (2021).
- [46] Guanze Liu, Yu Rong, and Lu Sheng. 2021. VoteHMR: Occlusion-Aware Voting Network for Robust 3D Human Mesh Recovery from Partial Point Clouds. In *Proceedings of the 29th ACM International Conference on Multimedia*. 955–964.
- [47] Yuan Liu, Zehong Shen, Zhixuan Lin, Sida Peng, Huijun Bao, and Xiaowei Zhou. 2019. Gift: Learning transformation-invariant dense visual descriptors via group cnns. In *NeurIPS*.
- [48] Fan Lu, Guang Chen, Yinlong Liu, Zhongnan Qu, and Alois Knoll. 2020. RSKDD-Net: Random Sample-based Keypoint Detector and Descriptor. In *NeurIPS*.
- [49] Weixin Lu, Guowei Wan, Yao Zhou, Xiangyu Fu, Pengfei Yuan, and Shiyu Song. 2019. DeepVCP: An End-to-End Deep Neural Network for Point Cloud Registration. In *ICCV*.
- [50] Bilawal Mahmood and SangUk Han. 2019. 3D registration of indoor point clouds for augmented reality. In *Computing in Civil Engineering 2019: Visualization, Information Modeling, and Simulation*. American Society of Civil Engineers Reston, VA, 1–8.
- [51] Marlon Marcon, Riccardo Spezialetti, Samuele Salti, Luciano Silva, and Luigi Di Stefano. 2021. Unsupervised Learning of Local Equivariant Descriptors for Point Clouds. *IEEE Transactions on Pattern Analysis and Machine Intelligence* 01 (2021), 1–1.
- [52] Niloy J Mitra and An Nguyen. 2003. Estimating surface normals in noisy point cloud data. In *Proceedings of the nineteenth annual symposium on Computational geometry*. 322–328.
- [53] Raul Mur-Artal, Jose Maria Martinez Montiel, and Juan D Tardos. 2015. ORB-SLAM: a versatile and accurate monocular SLAM system. *IEEE transactions on robotics* 31, 5 (2015), 1147–1163.
- [54] Richard A Newcombe, Shahram Izadi, Otmar Hilliges, David Molyneaux, David Kim, Andrew J Davison, Pushmeet Kohi, Jamie Shotton, Steve Hodges, and Andrew Fitzgibbon. 2011. Kinectfusion: Real-time dense surface mapping and tracking. In *2011 10th IEEE international symposium on mixed and augmented reality*. IEEE, 127–136.
- [55] G Dias Pais, Srikumar Ramalingam, Venu Madhav Govindu, Jacinto C Nascimento, Rama Chellappa, and Pedro Miraldo. 2020. 3DRegNet: A deep neural network for 3d point registration. In *CVPR*.
- [56] Liang Pan, Zhongang Cai, and Ziwei Liu. 2021. Robust Partial-to-Partial Point Cloud Registration in a Full Range. *arXiv preprint arXiv:2111.15606* (2021).
- [57] Adrien Poulenard and Leonidas J Guibas. 2021. A Functional Approach to Rotation Equivariant Non-Linearities for Tensor Field Networks. In *Proceedings of the IEEE/CVF Conference on Computer Vision and Pattern Recognition*. 13174–13183.

- [58] Adrien Poulenard, Marie-Julie Rakotosaona, Yann Ponty, and Maks Ovsjanikov. 2019. Effective rotation-invariant point CNN with spherical harmonics kernels. In *3DV*.
- [59] Charles R Qi, Hao Su, Kaichun Mo, and Leonidas J Guibas. 2017. PointNet: Deep learning on point sets for 3d classification and segmentation. In *CVPR*.
- [60] Zhijian Qiao, Zhe Liu, Chuanzhe Suo, Huanshu Wei, Zhuowen Shen, and Hesheng Wang. 2020. End-to-End 3D Point Cloud Learning for Registration Task Using Virtual Correspondences. In *IROS*.
- [61] Szymon Rusinkiewicz. 2019. A symmetric objective function for ICP. *ACM Transactions on Graphics (TOG)* 38, 4 (2019), 1–7.
- [62] Radu Bogdan Rusu, Nico Blodow, and Michael Beetz. 2009. Fast Point Feature Histograms (FPFH) for 3D registration. In *ICRA*.
- [63] Samuele Salti, Federico Tombari, and Luigi Di Stefano. 2014. SHOT: Unique signatures of histograms for surface and texture description. *Computer Vision and Image Understanding* 125 (2014), 251–264.
- [64] Wen Shen, Binbin Zhang, Shikun Huang, Zhihua Wei, and Quanshi Zhang. 2019. 3d-rotation-equivariant quaternion neural networks. *arXiv preprint arXiv:1911.09040* (2019).
- [65] Anthony Simeonov, Yilun Du, Andrea Tagliasacchi, Joshua B Tenenbaum, Alberto Rodriguez, Pulkit Agrawal, and Vincent Sitzmann. 2021. Neural Descriptor Fields: SE (3)-Equivariant Object Representations for Manipulation. *arXiv preprint arXiv:2112.05124* (2021).
- [66] Weiwei Sun, Andrea Tagliasacchi, Boyang Deng, Sara Sabour, Soroosh Yazdani, Geoffrey Hinton, and Kwang Moo Yi. 2021. Canonical Capsules: Unsupervised Capsules in Canonical Pose. In *NeurIPS*.
- [67] Xiao Sun, Zhouhui Lian, and Jianguo Xiao. 2019. Srinet: Learning strictly rotation-invariant representations for point cloud classification and segmentation. In *Proceedings of the 27th ACM International Conference on Multimedia*. 980–988.
- [68] Nathaniel Thomas, Tess Smidt, Steven Kearnes, Lusann Yang, Li Li, Kai Kohlhoff, and Patrick Riley. 2018. Tensor field networks: Rotation-and translation-equivariant neural networks for 3d point clouds. *arXiv preprint arXiv:1802.08219* (2018).
- [69] Yue Wang and Justin M Solomon. 2019. Deep Closest Point: Learning representations for point cloud registration. In *CVPR*.
- [70] Yue Wang and Justin M Solomon. 2019. PRNet: Self-supervised learning for partial-to-partial registration. In *NeurIPS*.
- [71] Yue Wang, Shusheng Zhang, Bile Wan, Weiping He, and Xiaoliang Bai. 2018. Point cloud and visual feature-based tracking method for an augmented reality-aided mechanical assembly system. *The International Journal of Advanced Manufacturing Technology* 99, 9 (2018), 2341–2352.
- [72] Svante Wold, Kim Esbensen, and Paul Geladi. 1987. Principal component analysis. *Chemometrics and intelligent laboratory systems* 2, 1-3 (1987), 37–52.
- [73] Daniel E Worrall, Stephan J Garbin, Daniyar Turmukhambetov, and Gabriel J Brostow. 2017. Harmonic Networks: Deep translation and rotation equivariance. In *CVPR*.
- [74] Jian Wu, Jianbo Jiao, Qingxiong Yang, Zheng-Jun Zha, and Xuejin Chen. 2019. Ground-aware point cloud semantic segmentation for autonomous driving. In *Proceedings of the 27th ACM International Conference on Multimedia*. 971–979.
- [75] Heng Yang, Jingnan Shi, and Luca Carlone. 2020. Teaser: Fast and certifiable point cloud registration. *IEEE Transactions on Robotics* 37, 2 (2020), 314–333.
- [76] Jiaolong Yang, Hongdong Li, Dylan Campbell, and Yunde Jia. 2015. Go-ICP: A globally optimal solution to 3D ICP point-set registration. *IEEE transactions on pattern analysis and machine intelligence* 38, 11 (2015), 2241–2254.
- [77] Hao Yu, Fu Li, Mahdi Saleh, Benjamin Busam, and Slobodan Ilic. 2021. CoFiNet: Reliable Coarse-to-fine Correspondences for Robust Point Cloud Registration. In *NeurIPS*.
- [78] Ruixuan Yu, Xin Wei, Federico Tombari, and Jian Sun. 2020. Deep Positional and Relational Feature Learning for Rotation-Invariant Point Cloud Analysis. In *ECCV*.
- [79] Wentao Yuan, Benjamin Eckart, Kihwan Kim, Varun Jampani, Dieter Fox, and Jan Kautz. 2020. DeepGMR: Learning Latent Gaussian Mixture Models for Registration. In *ECCV*.
- [80] Xiangyu Yue, Bichen Wu, Sanjit A Seshia, Kurt Keutzer, and Alberto L Sangiovanni-Vincentelli. 2018. A lidar point cloud generator: from a virtual world to autonomous driving. In *Proceedings of the 2018 ACM on International Conference on Multimedia Retrieval*. 458–464.
- [81] Andy Zeng, Shuran Song, Matthias Nießner, Matthew Fisher, Jianxiong Xiao, and Thomas Funkhouser. 2017. 3DMatch: Learning local geometric descriptors from rgb-d reconstructions. In *CVPR*.
- [82] Hongwen Zhang, Jie Cao, Guo Lu, Wanli Ouyang, and Zhenan Sun. 2019. Danet: Decompose-and-aggregate network for 3d human shape and pose estimation. In *Proceedings of the 27th ACM International Conference on Multimedia*. 935–944.
- [83] Zhiyuan Zhang, Yuchao Dai, and Jiada Sun. 2020. Deep learning based point cloud registration: an overview. *Virtual Reality & Intelligent Hardware* 2, 3 (2020), 222–246.
- [84] Yongheng Zhao, Tolga Birdal, Jan Eric Lenssen, Emanuele Menegatti, Leonidas Guibas, and Federico Tombari. 2020. Quaternion Equivariant Capsule Networks for 3d point clouds. In *ECCV*.
- [85] Dawei Zhong, Lei Han, and Lu Fang. 2019. iDFusion: Globally Consistent Dense 3D Reconstruction from RGB-D and Inertial Measurements. In *Proceedings of the 27th ACM International Conference on Multimedia*. 962–970.
- [86] Qian-Yi Zhou, Jaesik Park, and Vladlen Koltun. 2016. Fast Global Registration. In *ECCV*.
- [87] Qian-Yi Zhou, Jaesik Park, and Vladlen Koltun. 2018. Open3D: A modern library for 3D data processing. *arXiv preprint arXiv:1801.09847* (2018).
- [88] Minghan Zhu, Maani Ghaffari, and Huei Peng. 2022. Correspondence-free point cloud registration with SO (3)-equivariant implicit shape representations. In *Conference on Robot Learning*. PMLR, 1412–1422.

7 APPENDICES

A PROOF OF ROTATION EQUIVARIANCE

Rotation equivariance of f_0 . For an input neighboring point set N_p , its group feature f_0 can be written as:

$$f_0(g) = \varphi(T_g \circ N_p) \quad (11)$$

where φ is the FCGF backbone in YOHO. Using a rotation $m \in G$ in the icosahedral group to rotate the input point set, the corresponding group feature will become:

$$f'_0(g) = \varphi(T_g \circ T_m \circ N_p) \quad (12)$$

Due to the closure property of a group, the composition $gm \in G$, Eq. 12 can be expressed by

$$f'_0(g) = \varphi(T_{gm} \circ N_p) = f_0(gm) \quad (13)$$

Since f_0 is represented by a $60 \times n_0$ matrix and different row index represents different rotation $g \in G$, the g -th row on f'_0 will be equal to the gm -th row of f_0 , which means f'_0 is only a permuted version of f_0 , stated by

$$f'_0 = P_m \circ f_0 \quad (14)$$

where P_m is a permutation operator of $m \in G$.

Rotation equivariance of f_k . Here, we will prove that, if f_k is rotation-equivariant, which means $f'_k = P_m \circ f_k$, then the output feature f_{k+1} after the group convolution is also rotation-equivariant. We have the following results.

$$\begin{aligned} [f'_{k+1}(g)]_j &= \sum_i^{13} w_{j,i}^T f'_k(h_i g) + b_j \\ &= \sum_i^{13} w_{j,i}^T f_k(h_i gm) + b_j \\ &= [f_{k+1}(gm)]_j. \end{aligned} \quad (15)$$

The first equation is the definition of the group convolution. The second equation holds because $f'_k(g) = f_k(gm)$. The third equation also uses the definition of the group convolution which treats gm as a whole element. Since $f'_{k+1}(g) = f_{k+1}(gm)$ holds for any $g \in G$, $f'_{k+1} = P_m \circ f_{k+1}$.

B IMPLEMENTATION DETAILS

Training details for YOHO. The backbone, Group Feature Embedder and Rotation Residual Regressor are trained sequentially. First, we train the backbone FCGF under the same setting as [12] for 80 epochs but only use the rotation data argumentation in $[0^\circ, 50^\circ]$. Then, we train the group feature embedder for 10 epochs with a batch size of 32 with all rotation data augmentation of all angles. The training uses the Adam optimizer with a learning rate of $1e-4$. The learning rate is exponentially decayed by a factor of 0.5 every 1.8 epoch. Then, the following Rotation Residual Regressor is trained for 10 epochs with the same settings as the YOHO-Desc except that the origin learning rate is $1e-3$ and the decay step is 3 epochs.

Evaluation details. All baselines are evaluated using their official codes and models. Only the estimated correspondences are used for the inlier counting in both two modified RANSAC, same as [3].

C COMPARISON WITH DIRECT REGISTRATION METHODS

We further compare YOHO with methods designed specifically for direct registration of partial point clouds, i.e., Go-ICP [76], FGR [86], TEASER [75], PointNetLK [4], 3DRegNet [55], DGR [11], DHV [39], and PointDSC [6]. Following [6, 39], we report the percentage of successful alignment on 3DMatch and 3DLoMatch datasets in Table. 7, where one registration result is considered successful if the rotation error and translation error between the predicted and ground truth transformation are less than 15° and 0.3m. It can be observed that YOHO outperforms the direct registration methods on both datasets. Note that YOHO, as a descriptor, is not in conflict with these methods. These direct registration methods aim to directly estimate transformations on vanilla correspondences while the idea of YOHO is to associate a rotation on every vanilla correspondence. It would be an interesting topic to design new direct registration methods to process such rotation-associated correspondences in future works.

	3DMatch	3DLoMatch
Go-ICP [76]	22.90	-
FGR [86]	78.56	-
TEASER [75]	85.77	-
PointNetLK [4]	1.61	-
3DRegNet [55]	77.76	-
DGR [11]	86.50	50.20
DHV [39]	91.40	64.60
PointDSC [6]	93.28	61.50
YOHO-C	<u>93.30</u>	<u>66.40</u>
YOHO-O	93.47	67.20

Table 7: Comparison with direct registration methods on the 3DMatch and the 3DLoMatch datasets. The results in the table excluding ours are taken from PointDSC [6] and DHV [39].

Dataset	FMR (%)	IR (%)	#Iters	RR (%)
3DMatch	72.7	28.4	50k	48.3
3DLoMatch	28.2	5.7	50k	14.8
ETH	53.8	11.4	50k	47.2

Table 8: Performance of the PointNet backbone. All the metrics are computed with $\tau_c=0.1m$ and $\tau_r=0.2m$.

Dataset	FMR (%)	IR (%)	RR-C (%)	RR-O (%)	T-C (min)	T-O (min)
3DMatch	94.7	37.5	83.1	83.4	142.8	151.4
3DLoMatch	59.2	11.3	48.8	50.1		
ETH	85.4	12.8	97.8	89.8	44.2	46.6

Table 9: Results of YOHO-PN with 1k RANSAC iterations. All the metrics are computed with $\tau_c=0.1m$ and $\tau_r=0.2m$. ‘-C’ means the results of YOHO-C, ‘-O’ means the results of YOHO-O. T is the total time cost on the 3DMatch/3DLoMatch datasets or the ETH dataset.

D POINTNET AS BACKBONE

We train YOHO with a backbone of a simple 10-layer PointNet (YOHO-PN) processing a randomly sampled 1024-point local patch with the same radius selection as [3, 31]. We follow the same training settings as above to train the model. To avoid the rotation ambiguities, we filter out the planar keypoints by a simple threshold (≥ 0.03) on the minimum eigenvalue calculated by PCA [72]. The origin performances of the PointNet are shown in Table 8. The results of YOHO-PN are shown in Table 9.

From the results in Table 8 with Table 9 and the performance of baseline methods in the main paper, we can see that: (1) YOHO-PN brings great improvements to the simple PN backbone. (2) Even with a simple backbone, YOHO-PN already outperforms baselines [7, 12, 31, 43] in terms of RR. (3) As discussed in the ETH result section, since YOHO-PN does not need to downsample the point cloud, YOHO-PN achieves better FMR/IR than YOHO-FCGF in the strict setting with $\tau_c = 0.1m$ and $\tau_r = 0.2m$, which is comparable to SpinNet. Meanwhile, in terms of RR, YOHO-PN-C outperforms all baselines including SpinNet in this strict setting. (4) As a local patch based descriptor, YOHO-PN still costs less time than other local patch based descriptors SpinNet [3] and PerfectMatch [31].

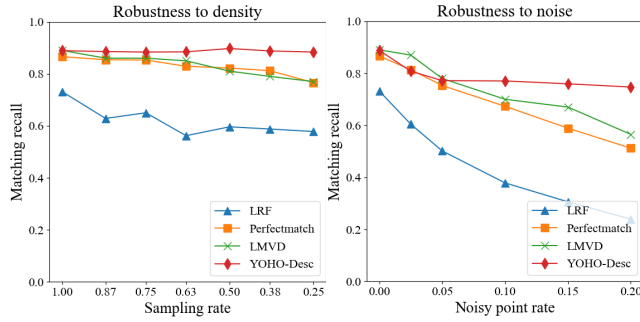


Figure 10: Ratio of correct patch pairs (y-axis) versus different levels of density and noise. In the experiment of density, we randomly drop some points in the patch and the x-axis shows the ratio of retained points. In the experiment of noise, we randomly add some noisy points to each patch where the x-axis shows the ratio of noisy points to the total point number.

E ROBUSTNESS ANALYSIS

To further verify the robustness of YOHO to point density and noise, we conduct an experiment using YOHO-PN. We synthesize a dataset based on the 3DMatch dataset by randomly sampling 3000 patch pairs. Each of which contains 40% points in a radius of 0.3m. We manually add random rotations and different levels of noise and density variations to every point cloud.

We compare the invariance from the proposed YOHO-PN with the (1) PCA+PointNet which achieves rotation invariance from PCA, (2) PerfectMatch [31] which achieves rotation invariance from plane fitting and (3) LMVD [43] which achieves rotation invariance from multi-view images on the local point patch. We report the ratio of correct patch pairs, i.e. matching recall, found by all descriptors. The results are shown in Fig 10. With the decreasing of the

density and increasing of noise, the performance of YOHO-Desc almost stays the same or drops much slowly comparing with baselines, which demonstrates the robustness of our rotation-invariance construction.

F RESULTS ON THE WHU-TLS DATASET

We further provide the results of our model on the WHU-TLS[21] dataset with $\tau_c = 0.5m$ and $\tau_r = 1m$ using 5000 keypoints, as shown in Table 10. For SpinNet[3], we change the patch radius from 2m to 6m and choose the best results. For YOHO-PN, the patch radius is set to 6m. For YOHO, the downsample voxelsize is set to 0.8m. The results show that YOHO also generalizes better to the unseen WHU-TLS dataset than SpinNet.

Scenes	Prk	Mnt	Cmp	Riv	Cav	Tun	Avg
Feature Matching Recall (%)							
SpinNet[3]	22.6	0.0	0.0	0.0	36.4	0.0	9.8
YOHO-PN	96.8	100.0	33.3	33.3	90.9	16.7	61.8
YOHO	<u>93.5</u>	100.0	44.4	<u>16.7</u>	<u>81.8</u>	<u>16.7</u>	<u>58.9</u>
Inlier Ratio (%)							
SpinNet[3]	4.3	0.0	1.4	0.1	5.1	0.0	1.8
YOHO-PN	13.6	<u>10.3</u>	<u>4.2</u>	5.0	15.6	2.7	8.6
YOHO	<u>13.2</u>	11.0	5.5	4.0	<u>11.2</u>	<u>1.4</u>	<u>7.7</u>
Registration Recall (%)							
SpinNet[3]	80.6	0.0	44.4	0.0	9.1	0.0	22.4
YOHO-PN-C	90.3	100.0	88.9	16.7	<u>18.2</u>	<u>16.7</u>	55.1
YOHO-PN-O	77.4	20.0	55.5	0.0	0.0	33.3	31.0
YOHO-C	<u>87.1</u>	100.0	<u>77.8</u>	0.0	27.3	<u>16.7</u>	<u>51.5</u>
YOHO-O	80.6	<u>80.0</u>	44.4	0.0	9.1	<u>16.7</u>	38.5
YOHO-PN-C+ICP	100	100	88.9	100	90.9	16.7	82.8
YOHO-PN-O+ICP	100	100	77.8	83.3	90.9	33.3	80.9
YOHO-C+ICP	100	100	88.9	100	81.8	16.7	<u>81.2</u>
YOHO-O+ICP	100	100	77.8	100	81.8	16.7	79.4

Table 10: Detailed results on the WHU-TLS dataset of different scenes.

G COMPARISON WITH EPN [10]

YOHO differs from EPN on two parts. The most different part is that when aligning partial scans like 3DMatch, YOHO propose a novel framework that takes use of the estimated rotation in the modified RANSAC to improve its accuracy and efficiency while EPN solely relies on rotation-invariant descriptors to build putative correspondences and adopts a vanilla RANSAC. The second difference is that EPN proposes a neat and efficient $SE(3)$ convolution layer, which decomposes $SE(3)$ into two groups and applies point convolutions and group convolutions in turns. However, EPN still relies features defined on the whole $SE(3)$ space, which means they need to retain the icosahedral group features on all points and every $SE(3)$ convolution layer involves icosahedral group features of all points. In comparison, YOHO first relies a backbone to extract the patterns defined on points and then we only consider the icosahedral group features for specific keypoints, which greatly reduce the computation burdens. Meanwhile, separating features extraction on points and icosahedral group also enables YOHO to adopt the computation-efficient backbone like FCGF [12]. Our experiments demonstrate our superior performance over EPN especially in terms of computational efficiency.